All-Digital Impulse Radio With Multiuser Detection for Wireless Cellular Systems

Christophe J. Le Martret and Georgios B. Giannakis, *Fellow, IEEE*

***Abstract*—Impulse radio is an ultrawideband system with attractive features for baseband asynchronous multiple-access, multimedia services, and tactical wireless communications. Implemented with analog components, the continuous-time impulse radio multiple-access model utilizes pulse-position modulation and random time-hopping codes to alleviate multipath effects and suppress multiuser interference. We introduce a novel continuous-time impulse radio transmitter model and deduce from it an approximate one with lower complexity. We also develop a time-division duplex access protocol along with orthogonal user codes to enable impulse radio as a radio link for wireless cellular systems. Relying on this protocol, we then derive a multiple-input/multiple-output equivalent model for full continuous-time model and a single-input/single-output model, for the approximate one. Based on these models, we finally develop design composite linear/nonlinear receivers for the downlink. The linear step eliminates multiuser interference deterministically and accounts for frequency-selective multipath while a maximum-likelihood receiver performs symbol detection. Simulations are provided to compare performance of the different receivers.**

***Index Terms*—Impulse radio, multipath fading channels, time-division duplex, ultrawideband systems, wireless cellular systems.**

I. Introduction

THE IDEA of transmitting digital information using ultrashort impulses was first presented in [1] and called *Impulse Radio* (IR). It relies on pulse-position modulation (PPM) and time diversity that is gained by repeating the same symbol many ($\geq$ 1000) times, according to a random code, which embodies IR with a very high processing gain. The attractive features of IR can be summarized as follows: it transmits at baseband and thus no intermediate frequency nor carrier synchronization processing is needed; it consumes minimal power; and, it is robust against jamming and multipath. IR has also been extended to multiuser communications in [2], where it is known as impulse radio multiple-access (IRMA). Its principle is based on asynchronous user transmissions and statistical multiuser interference (MUI) suppression that relies on power control.

Paper approved by M. Z. Win, the Editor for Equalization and Diversity of the IEEE Communications Society. Manuscript received May 24, 2000; revised September 18, 2001 and February 20, 2002. This paper was presented in part at the 1st Sensor Array and Multichannel Signal Processing Workshop, Boston, MA, March 2000, and at the MILCOM'00 Conference, Los Angeles, CA, October 2000.

C. J. Le Martret is with THALES Communications France, TRS/TSI, 92231 Genneviliers Cedex, France (e-mail: christophe.le_martret@fr.thales-group.com).

G. B. Giannakis is with the Department of Electrical and Computer Engineering, University of Minnesota, Minneapolis, MN 55455 USA (e-mail: georgios @ ece.umn.edu).

Publisher Item Identifier 10.1109/TCOMM.2002.802559.

Subsequent works have focused on optimizing the efficiency of IRMA by characterizing the channel [3]–[5], improving the modulation format [6], [7] and addressing networking aspects [8], [9]. Recently, an application of IRMA has been considered in [10] for the radio link in a multimedia PCS communication scenario.

The aim of this work is to explore usage of the IR concept as the radio link in a wireless cellular setting that consists of (micro-)cells with a few users (say less than 32). In all IRMA schemes proposed so far, the interference due to other users is randomized and only statistically suppressed, provided that (strict) power control is successfully applied. This solution may be well motivated for ad hoc architectures, but prevents one from taking advantage of multiuser detection (MUD). Indeed, the latter brings benefits over the statistical MUI cancellation when the number of users is small and thus the independent Gaussian approximation of the interference is no longer valid. MUD alleviates the need for power control and facilitates channel equalization to mitigate multipath effects. Equalization has not been explicitly addressed for conventional IR systems. On the other hand, based on a pragmatic propagation model, it has been verified recently that IR performance degrades severely if multipath effects are not accounted for [11]. RAKE reception offers an option, but its complexity increases when more than 50 fingers are required for reliable performance [3], [5]. Zero-forcing (ZF) or minimum mean-square error (MMSE) equalizers outperform RAKE receivers and their digital implementations are well motivated for IR.

To apply MUD to IRMA, we first present a new continuous-time model for the PPM-IRMA scheme (Section II). This model is realizable by parallel linear modulators whose inputs can be expressed as the output of a spreading operator, that is fed by a nonlinear transformation of the symbols. Based on this model, we then derive an approximate model that affords a simpler transmitter design but requires sampling faster than the chip rate. When the period of the pseudorandom hopping sequence is an integer multiple of the number of frames per symbol, the spreading operator can be implemented using filterbanks.

Next, we develop a time-division duplex (TDD) protocol to enable IRMA operation in a wireless cellular environment. Our protocol relies on orthogonal code designs and it is based on alternate slotted transmissions between users and the base station (BS) (Section III). We address the problem of time synchronization with the BS through guard times that ensure nonoverlapping transmissions.

Relying on the TDD protocol, we pursue then an all-digital IRMA transmission model that is equivalent to the

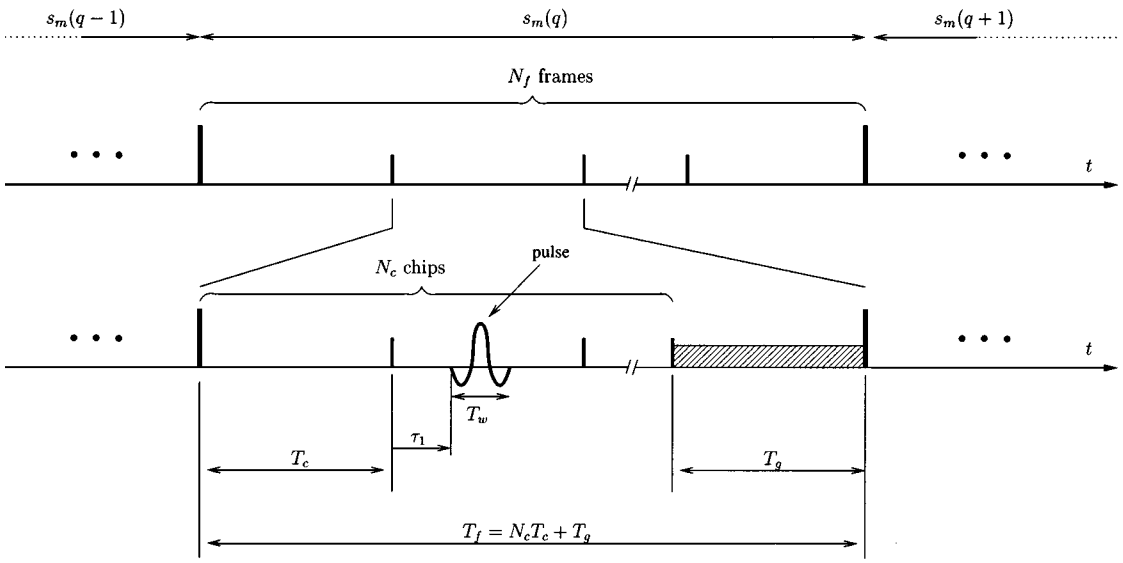

Fig. 1. Time scale representation of the different parameters in the IRMA (1) for the qth symbol of user m. The zoom on the second frame shows the pulse placed in the second chip ($\tilde{c}_m(k) = 2$) and shifted by τ_1 ($s_m(q) = 1$).

continuous-time one and can be represented in discrete-time as a multiple-input/multiple-output (MIMO) system (Section IV-A). We present also the discrete-time model derived from the approximate one which has a simpler receiver structure and turns out to be single-input/single-output (SISO) (Section IV-B).

Based on the discrete-time modeling, we propose three digital receivers for the downlink of an IRMA cellular system for both MIMO and SISO models (Section V). They are composed of a linear filter for channel mitigation and user separation, followed by a maximum-likelihood (ML) detector for symbol recovery.

Finally, we derive a symbol error rate (SER) bound for the zero forcing receiver and provide simulations of the different receivers in a multiuser, frequency selective multipath propagation environment (Section VI).

II. Continuous-Time PPM-IRMA

To introduce notation and facilitate the transition from the original continuous-time PPM to our novel model, we first review the conventional PPM-IRMA briefly.

A. Conventional PPM-IRMA Modeling

In PPM-IRMA, each user (say the mth) transmits each information symbol $s_m(q)$ drawn from the alphabet $\{0, 1, \ldots, A-1\}$ repeatedly over N_f frames each of duration T_f. Specifically, letting the frame index to be $k = qN_f + r$, $r \in [0, N_f - 1]$ and with $\lfloor x \rfloor$ denoting integer-floor, the qth symbol can be written as: $s_m(q) = s_m(\lfloor k/N_f \rfloor)$. The same signal $s_m(\lfloor k/N_f \rfloor)$ is transmitted N_f times using a position-hopping sequence $\tilde{c}_m(k)$ having N_c possible hops (chips) per frame. With T_c denoting chip duration, we thus have $T_f = N_cT_c + T_g$, where T_g is a guard time introduced to account for processing delay at the receiver between two successive received frames (see, e.g., [10]). For the kth frame and depending on the value $n_c \in [0, N_c-1]$ of the code $\tilde{c}_m(k) = n_c$, the chip-pulse (also known as the monocycle) $w(t)$ of duration $T_w \ll T_c$, is positioned at the n_cth chip interval. Within this chip interval, the monocycle is shifted by $\tau_{s_m(q)}$ to implement the PPM with $0 \leq \tau_{s_m(q)} < T_c - T_w$. With these notational conventions, the mth user's transmitted waveform is given by (see, e.g., [6])

$$v_m(t) = \mathcal{P} \sum_{k=-\infty}^{+\infty} w\left(t - kT_f - \tilde{c}_m(k)T_c - \tau_{s_m(\lfloor k/N_f \rfloor)}\right) \quad (1)$$

where $\mathcal{P}$ is the amplitude which controls the transmitted power. The code $\tilde{c}_m(k)$ is a periodic pseudorandom sequence [2] with period $P_{\tilde{c}}$. Fig. 1 illustrates the time scale representation of the parameters in IR.

B. Novel PPM-IRMA Modeling

We present here a novel model for the IR that relies on the fact that the PPM signal can be expressed as the sum of linear modulators, fed by a nonlinear transformation of the information symbols. In each segment of duration $N_fN_cT_c$ corresponding to N_f repetitions of a single symbol, the pulse stream is shifted in time according to the symbol value; e.g., it is shifted by τ_a, if $s_m(q) = a$. One way to model this is to have A parallel branches, each realizing a shifted version of the pulse stream. In order to generate the signal, we then only need to select one branch out of A depending on the symbol value. Adopting this viewpoint and defining $s_{m,k} := s_m(\lfloor k/N_f \rfloor)$, we can re-express (1) as

$$v_m(t) = \sum_{a=0}^{A-1} v_{m,a}(t) \quad (2)$$

with

$$v_{m,a}(t) = \mathcal{P} \sum_{k=-\infty}^{+\infty} \beta_a(s_{m,k})\, w\left(t - kT_f - \tilde{c}_m(k)T_c - \tau_a\right) \quad (3)$$

where $\beta_a(\cdot)$ captures the branch selection process according to the following definition:

$$\text{for } s, a \in [0, A-1], \quad \beta_a(s) := \begin{cases} 1, & \text{if } s = a \\ 0, & \text{otherwise.} \end{cases} \tag{4}$$

Hence, by defining the time-shifted pulses $w_a(t) := w(t - \tau_a)$ and recalling that $T_f = N_c T_c$ for $T_g = 0$, (3) can be rewritten as

$$v_{m,a}(t) = \mathcal{P} \sum_{k=-\infty}^{+\infty} \beta_a(s_{m,k})\, w_a(t - (kN_c + \tilde{c}_m(k))\, T_c). \tag{5}$$

Because $\tilde{c}_m(k) = n_c$ and n_c is an integer in $[0, N_c - 1]$, we infer that $w_a(t)$ in (5) is shifted by an integer multiple of T_c. It is thus possible to view $v_{m,a}(t)$ as a linearly modulated waveform with symbol rate $1/T_c$, and express it as

$$v_{m,a}(t) = \mathcal{P} \sum_{n=-\infty}^{+\infty} u_{m,a}(n) w_a(t - nT_c) \tag{6}$$

where $u_{m,a}(n)$ is a sequence that depends on $s_m(k)$ and $\tilde{c}_m(k)$. Thus, (2) can be interpreted as the superposition of A linear modulators each with a different pulse function $w_a(t)$.

Note that the index k in (5) denotes the frame number while n in (6) corresponds to the chip index across the frame. Because these two indices are related by $n = kN_c + r$ with $r \in [0, N_c - 1]$, we deduce that $u_{m,a}(n) = \beta_a(s_m(\lfloor k/N_c \rfloor))c_m(n)$, where $c_m(n) = \delta(r - \tilde{c}_m(\lfloor n/N_c \rfloor))$ and $\delta(\cdot)$ denotes Kronecker's delta. Observing that $r = n - kN_c = n - \lfloor n/N_c \rfloor N_c$, the latter can be written as

$$c_m(n) = \begin{cases} 1, & \text{if } \tilde{c}_m\left(\left\lfloor \frac{n}{N_c} \right\rfloor\right) = n - \left\lfloor \frac{n}{N_c} \right\rfloor N_c \\ 0, & \text{otherwise.} \end{cases} \tag{7}$$

To express the generic qth symbol $s_m(q)$ in terms of the chip index n, we recall that $k = \lfloor n/N_c \rfloor$ and $q = \lfloor k/N_f \rfloor$, which imply that $q = \lfloor n/(N_c N_f) \rfloor$. Substituting the latter in our expression for $u_{m,a}(n)$, we arrive at

$$u_{m,a}(n) := \beta_a\left(s_m\left(\left\lfloor \frac{n}{N_c N_f} \right\rfloor\right)\right) c_m(n). \tag{8}$$

Hence, the continuous-time PPM-IRMA transmission can be depicted as in Fig. 2, where the notation $S(c_m)$ stands for the spreading operation defined by (8).

If the hopping code $\tilde{c}_m(n)$ has period $P_{\tilde{c}}$, then it can be readily verified by direct substitution that the period of $c_m(n)$ in (7) is $P_c = N_c P_{\tilde{c}}$. To illustrate the link between $\tilde{c}_m(n)$ and $c_m(n)$ with an example, let us consider $K = 4$, $N_f = 2$, $N_c = 3$ and $\tilde{c}_m(n) = \{11200210\}$. Using (7), we then find $c_m(n) = \{010010001100100001010100\}$ [see also Fig. 3(a)].

Unlike the conventional model, we have assumed here for simplicity that $T_g = 0$. In fact, our novel model can encompass the case $T_g \neq 0$ as well, by setting $T_g = N_g T_c$, with N_g integer and restricting the sequence $\tilde{c}_m(n)$ to take its values in $[0, N_c' - 1]$, where $N_c' := N_c - N_g$.

C. Approximate Chip-Oversampled PPM-IRMA Model

With reference to the continuous-time model of Fig. 2, we develop here an approximate chip-oversampled discrete-time model of PPM-IRMA by moving the time-shifted form of the PPM pulse-shaper $w_a(t)$ to the spreading code itself. The outputs $u_{m,a}(n)$ for $0 < a < A$ will then be delayed versions of $u_{m,0}(n)$ and only one transmit filter will be sufficient. The price paid for such a simplification is increase in the transmitted symbol rate in order to realize subchip delays $\tau_a < T_c$. Parsing the chip length into N_τ segments, the new symbol rate becomes $1/T_\tau$, with $T_\tau = T_c/N_\tau$. The approximation stems from the fact that the real delays τ_a are approximated by integer delays $d_a := \text{round}[\tau_a/T_\tau]$. Certainly, we can render the rounding error as small as we wish by choosing N_τ sufficiently large.

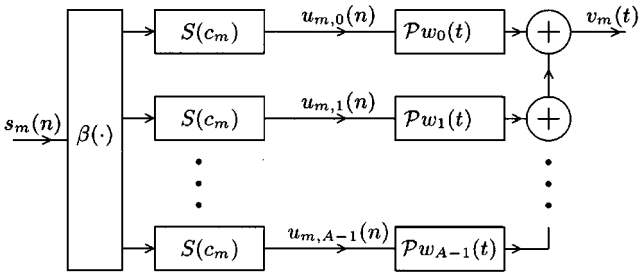

Fig. 2. Continuous-time PPM-IRMA model (mth user).

The spreading implementation can accommodate the approximate model by simply inserting $N_\tau - 1$ zeros between successive chips of the sequences $c_m(n)$.

If $\bar{c}_m(n)$ denotes the new code sequence, we have

$$\bar{c}_m(n) = c_m\left(\left\lfloor \frac{n}{N_\tau} \right\rfloor\right) \delta\left(n - N_\tau \left\lfloor \frac{n}{N_\tau} \right\rfloor\right). \tag{9}$$

The approximate modeling is depicted in Fig. 4, where the delayed filterbank precoder outputs are defined as

$$\bar{u}_{m,a}(n) := \beta_a\left(s_m\left(\left\lfloor \frac{n - d_a}{N_c N_f N_\tau} \right\rfloor\right)\right) \bar{c}_m(n - d_a). \tag{10}$$

Based on (10), we can then define

$$\bar{u}_m(n) := \sum_{a=0}^{A-1} \bar{u}_{m,a}(n) \tag{11}$$

to obtain the transmitted signal for the chip-oversampled PPM-IRMA transmissions as

$$\bar{v}_m(t) = \mathcal{P} \sum_{n=-\infty}^{+\infty} \bar{u}_m(n) w(t - nT_\tau). \tag{12}$$

D. Filterbank Implementation of IRMA With Block-Periodic Codes

If we restrict the time hopping sequence period to be an integer multiple of the number of frames, i.e., $P_{\tilde{c}} = KN_f$, we will see that the spreading can be implemented using filterbanks. Such a *block-periodic* code that will be adopted henceforth, implies a block spreading operation where each block of K information bearing symbols $\{s_m(qK), s_m(qK+1), \ldots, s_m((q+1)K-1)\}$ is spread by the same hopping sequence over KN_f frames. The block-periodic code structure will prove useful in developing our digital receivers. The parameter K can be easily adjusted and will turn out to be the number of transmitted symbols per burst in the TDD protocol of Section III-A.

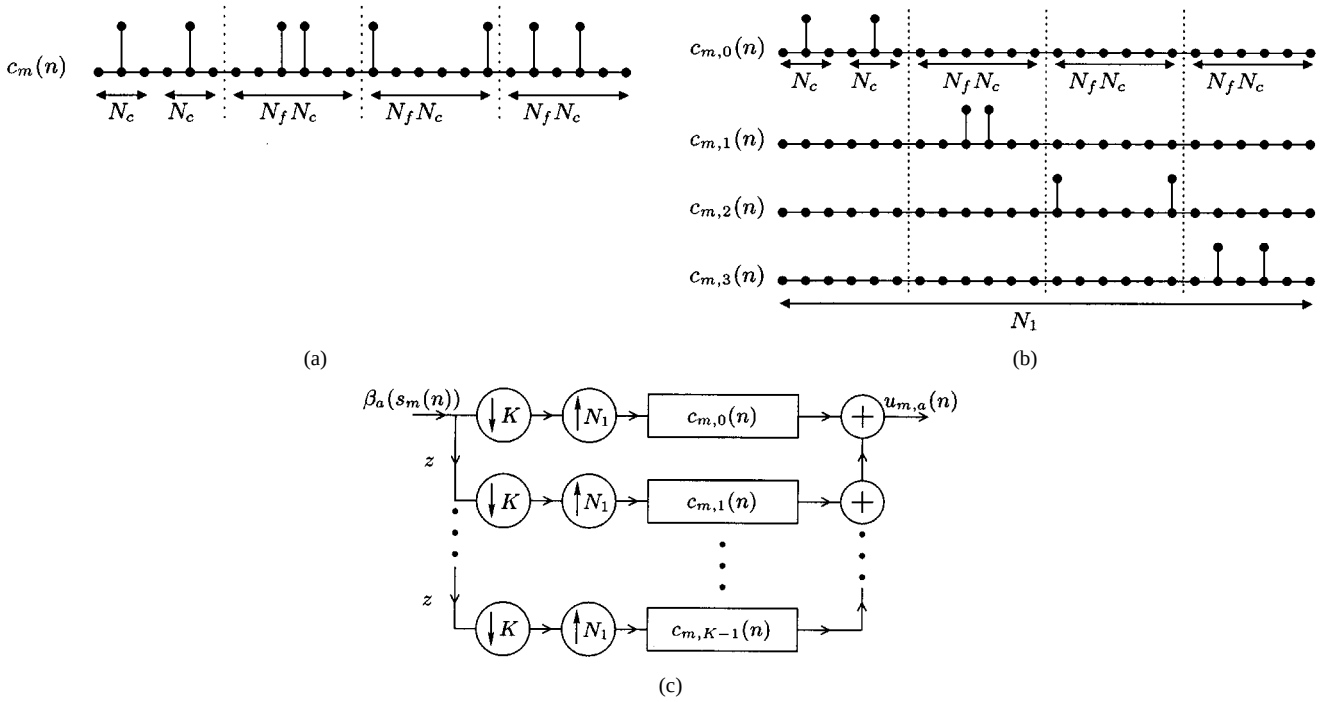

Fig. 3. Code sequences for the novel PPM-IRMA model. (a) $c_m(n) = \{0100100011001000010101 00\}$ obtained from $\bar{c}_m(n) = \{11200210\}$ for $K = 4$, $N_f = 2$ and $N_c = 3$. (b) Codes $c_{m,k}(n)$ deduced from $c_m(n)$ for filterbank implementation. (c) Filterbank implementation of the PPM-IRMA spreading for branch a ($N_1 = KN_fN_c$).

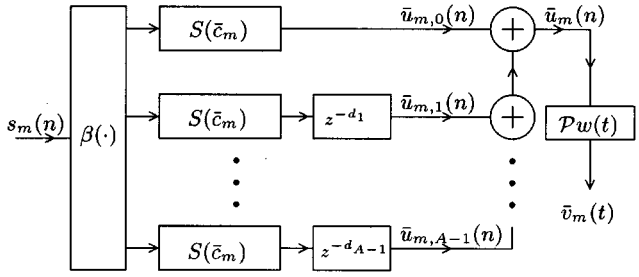

Fig. 4. Approximate continuous-time PPM-IRMA model (mth user).

Because $c_m(n)$ in (7) has period P_c and is spread over K symbols, it is convenient to express $u_m(n)$ in block form with the ith transmitted block of size P_c denoted as $u_{m,a}(i;p)$ after setting $n = iP_c + p$ with $p = kN_cN_f + q$, $p \in [0, P_c - 1]$, and $q \in [0, N_cN_f - 1]$. We can then use (8) to obtain $u_{m,a}(i;p) = \beta_a(s_m(iK + k))c_m(p)$. Recall now that $k \in [0, K - 1]$ when $p \in [0, P_c - 1]$ and k remains constant over N_fN_c chips. Hence, the ith transmitted block is given by [cf. (8)]

$$u_{m,a}(i;p) = \sum_{k=0}^{K-1} \beta_a\left(s_m(iK+k)\right) c_{m,k}(p) \qquad (13)$$

where $c_{m,k}(p)$ is defined as

$$c_{m,k}(p) = \begin{cases} c_m(p), & \text{for } kN_fN_c \le p \le (k+1)N_fN_c - 1 \\ 0, & \text{otherwise.} \end{cases} \qquad (14)$$

Using the same example as in Fig. 3(a) for the code $c_m(n)$, Fig. 3(b) depicts the code $c_{m,k}(n)$ with $N_1 := KN_fN_c$. From this perspective, our PPM-IRMA model can be viewed as a multicode CDMA system (see, e.g., [12] and [13]).

Expression (13) is identical to the one given in [14, eq. (1)], where it is shown that $u_m(i;p)$ is the output of the filterbank shown in Fig. 3(c). We thus infer that our PPM-IRMA transmitted sequence can also be implemented with a discrete-time filterbank.

The filterbank implementation can accommodate the approximate model of Section II-C by modifying the upsampling factor. Because the symbol rate is N_τ times that of the linear model (6), the upsampling factor becomes $N_1' := N_\tau N_1$.

We have presented a novel IRMA model and an approximate version of it. When the hopping sequence is block-periodic, we have shown that these models can be implemented using filterbanks which turns out to be very flexible when the models have to be adjusted to the transmission protocol of the next section. The block-periodic assumption does not modify the power spectral density of the IR signal since, as discussed in [15], the spectral lines are only affected by the value of the ratio T_f/T_c. Moreover, although the block-periodic assumption facilitates the implementation of the spreading operation by using filterbanks, the derivations in the rest of the paper can be generalized to any value of the time hopping period. In this case, the discrete-time equivalent model in Section IV and the digital receivers derived in Section V would have to be slightly modified accordingly (see discussion by the end of Section IV).

III. TDD IRMA

Unlike existing IRMA schemes that consider asynchronous transmissions through frequency-flat channels and suppress MUI statistically, we propose here a novel IRMA approach using orthogonal codes in a synchronous or quasi-synchronous

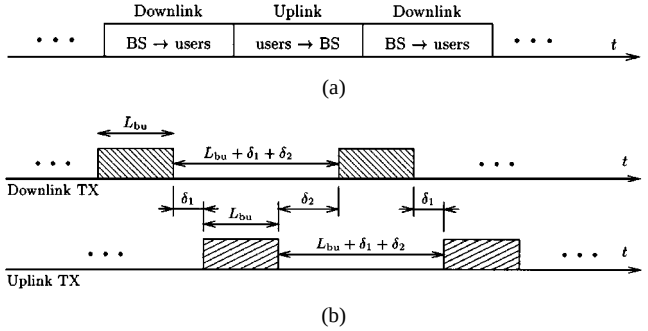

Fig. 5. TDD-IRMA slots. (a) Successive slots for TDD in uplink/downlink pairs. (b) Timing parameters for TDD-IRMA slots.

context, coupled with TDD for transmissions through frequency-selective channels. This is achieved by assigning to each user different orthogonal time-hopping sequences and designating two time slots for transmission: one for the uplink and one for the downlink.

A. TDD-IRMA Protocol

Because IR transmits at baseband, there is no carrier frequency and hence, we cannot use frequency-division duplexing (FDD) as in most multiuser systems. Here, we have to resort to TDD in order to provide a full duplex link between the users and the BS. Successive time slots in TDD are designated for the downlink and the uplink as shown in Fig. 5(a).

We assume that the users have a common time reference so that transmissions can essentially be considered as quasi-synchronous as in IS-95, where even in the uplink users attempt to synchronize with the pilot waveform broadcasted by the BS. The term quasi-synchronous means that although a time reference is present, small offsets arising due to the time jitter of each user's clock and relative propagation delays between the users and the base station, are allowed but must be accounted for.

Because of the block structure we have introduced in Section II, each IRMA user transmits K information symbols during one time slot, for both downlink and uplink sessions. Thus, the downlink transmitted signal is composed of a burst conveying MK symbols, where M is the maximum number of active users, followed by a silent interval (no signal) of approximately the same duration. Conversely for the uplink, each user sends K information symbols within the same time slot during the silent period of the downlink session and follows it up with a silent interval to enable the downlink burst transmission. The timing of these slots is represented in Fig. 5(b), where $L_{\rm bu}$ is the burst duration.

As depicted in Fig. 5(b), the slot has duration $L_{\rm bu} + \delta_1 + \delta_2$ with $\delta_1 > 0$ and $\delta_2 > 0$ and is thus longer than the burst. The timing offset δ_1 determines the time between the end of the BS burst and the beginning of the users' bursts, while δ_2 denotes the time between the end of the users' bursts and the beginning of the BS burst. These offsets are set to account for the asynchronism and also for the propagation channel. Let us define l_m to be the asynchronism between the BS and user m; L_m^u the channel length in the uplink between user m and the BS; and L_m^d the channel length in the downlink between the BS and user m. Clearly, the transmitted burst from the BS should not overlap in time with the received bursts sent by the users and vice versa.

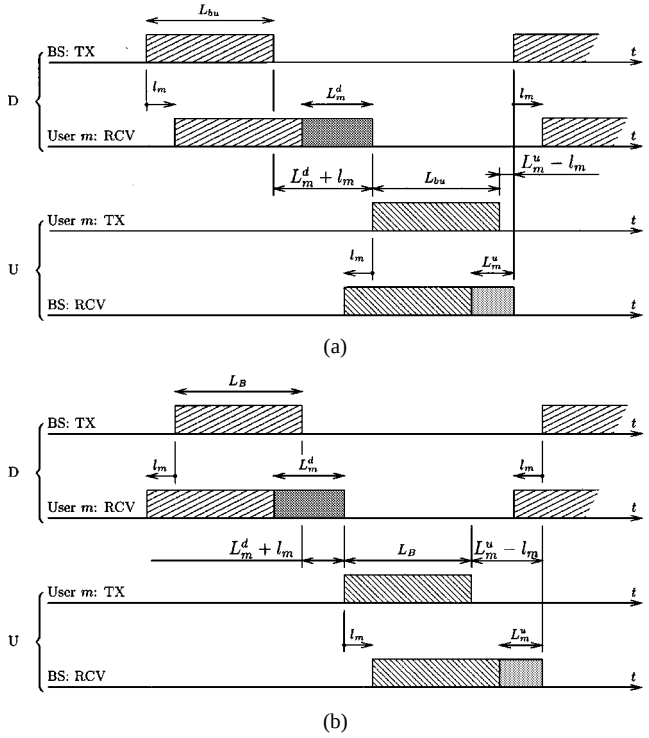

Fig. 6. Timing frames for the TDD-IRMA slots. (a) Case $l_m \geq 0$. (b) Case $l_m < 0$.

In order to select values for δ_1 and δ_2 which satisfy this condition, we will assume that the channel lengths L_m^u and L_m^d are larger (in absolute value) than the asynchronism l_m. This assumption, made for simplicity, is reasonable since every user has a time reference. The asynchronism l_m can have either positive or negative values. Moreover, in an absolute time reference, if the BS "sees" user m with delay l_m, then user m will "see" the base station with delay $-l_m$. Accordingly, we depict in Fig. 6 the timing structure of the different slots in the uplink and the downlink, for both positive and negative values of l_m. The same picture for negative values of l_m leads to the same expressions for guard-intervals δ_1 and δ_2. These values must be selected in order to handle the worst case scenario. Defining $\mathcal{D} := [0, M-1]$, the worst case can be accommodated by choosing

$$\delta_1 = \sup_{m \in \mathcal{D}} \left\{ L_m^d + l_m \right\}, \qquad \delta_2 = \sup_{m \in \mathcal{D}} \left\{ L_m^u - l_m \right\}. \quad (15)$$

For both the uplink and the downlink, the transmitted burst has duration $L_{\rm bu} = N_1 T_c$ seconds while the subsequent silent interval has duration $L_{\rm si} = N_1 T_c + \delta_1 + \delta_2$ seconds. In order to match the all-digital modeling, the different time intervals must be multiples of the sample duration. Thus, defining $L_1 := \lceil \delta_1 / T_c \rceil$ and $L_2 := \lceil \delta_2 / T_c \rceil$, where $\lceil x \rceil$ is the integer ceiling of x, the timing will be set to $\delta_1 = L_1 T_c$ and $\delta_2 = L_2 T_c$ which leads to a new silent duration of $L_{\rm si} = (N_1 + L) T_c$ seconds with $L := L_1 + L_2$.

For this protocol, K symbols per user are transmitted every $(L_{\rm bu} + L_{\rm si})$ seconds; thus, we deduce that the bit rate per user is given by (with alphabet size $A = 2^{q_A}$)

$$D = \frac{q_A K}{(2N_1 + L) T_c} \quad \text{(b/s)}. \quad (16)$$

We will now see how to design orthogonal codes for the different users to ensure deterministic MUI suppression at the receivers for the downlink.

B. Designing Orthogonal IRMA Codes

The digital models described in Section II can accommodate the silent signal portion by simply padding the code sequences with zeros. Since the silent period lasts N_1+L chips, the number of trailing zeros will be N_1+L and therefore the length of the codes becomes $N_3 := 2N_1+L$.

An orthogonal IRMA scheme capable of eliminating MUI in the downlink is possible by assigning to each user, one of the N_c chip positions in each of the KN_f frames, with none of the chips belonging to more than one user. This is equivalent to having orthogonal spreading sequences $c_m(n)$, where orthogonality is defined as follows.

Definition 1: Two code sequences $c_{m_1}(n)$ and $c_{m_2}(n)$ defined as in (7) are orthogonal if and only if $\mathbf{c}_{m_1}^T\mathbf{c}_{m_2}=0$, where $\mathbf{c}_{m_i}=[c_{m_i}(0),\ldots,c_{m_i}(N_1-1)]^T$ for $i=1,2$, and ^{T} stands for transpose.

To build such orthogonal codes, we recall (7) and establish the following equivalence.

Proposition 1: If according to (7), $\check{c}_{m_1}(n)$ and $\check{c}_{m_2}(n)$, have corresponding spreading sequences $c_{m_1}(n)$ and $c_{m_2}(n)$, then

$$\mathbf{c}_{m_1}^T\mathbf{c}_{m_2}=0 \Leftrightarrow \check{c}_{m_1}(n)\neq\check{c}_{m_2}(n), \qquad \forall n\in[0,KN_c-1]\,.$$

Because there are N_c chips per frame, we deduce that the maximum number of users we can accommodate is N_c. Using *Proposition 1*, we can define the set $\mathcal{C}$ of N_c orthogonal codes for the TDD-IRMA transmission scheme as

$$\mathcal{C}=\left\{\{\check{c}_m(n)\}_{m=0}^{N_c-1}:\mathbf{c}_{m_1}^T\mathbf{c}_{m_2}=0,\ \forall m_1\neq m_2\right\}. \quad (17)$$

With no other constraint than orthogonality (one can also use correlation constraints for synchronization purposes), a simple means of constructing sequences satisfying (17) is to generate them randomly, user after user, while checking for orthogonality.

IV. Discrete-Time Equivalent Model

We derive here the discrete-time equivalent model of the PPM-IRMA in the single-user case for simplicity. We first present in Section IV-A the MIMO model deduced from the model of Section II-B. Then we develop an approximate SISO model in Section IV-B which leads to a simplified receiver.

A. Chip-Sampled MIMO Model

The transmitted symbols are sent at a rate $1/T_c$ and we sample the received signal at the same rate. Adhering to PPM, this can only be achieved by passing the received signal through A parallel filters matched to the pulses $w_a(t)$ prior to sampling. We thus arrive at the MIMO continuous-time PPM-IRMA transmission model shown in Fig. 7.

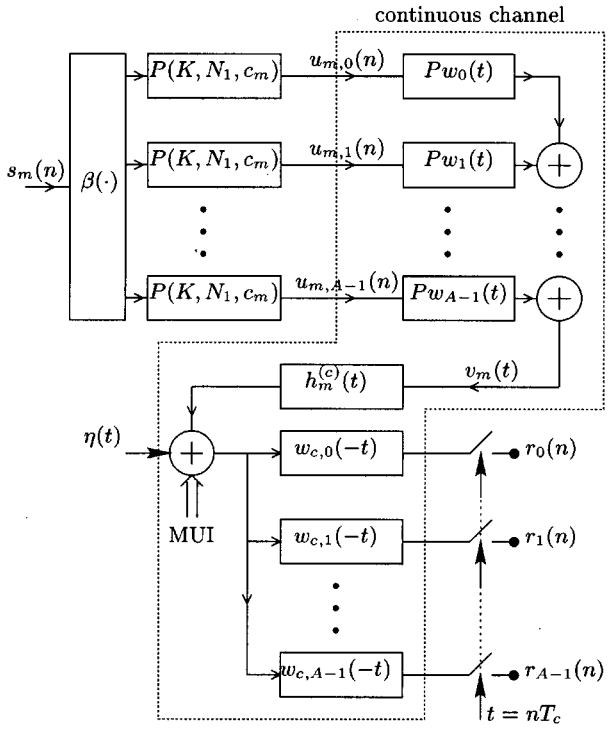

Fig. 7. MIMO PPM-IRMA model for the downlink (mth user receiver).

It follows from (2) and (6) that the chip-sampled matched filter output of the bth branch at the receiver is

$$y_{m,b}(n)=\mathcal{P}\sum_{a=0}^{A-1}\sum_{k=0}^{L_1}h_{m,b,a}(k)u_{m,a}(n-k)+\eta_b(n) \quad (18)$$

with $h_{m,b,a}(k):=w_a(t)\star h_m(t)\star w_b(-t)|_{t=kT_c}$ and $\eta_b(n):=\eta(t)\star w_b(-t)|_{t=nT_c}$ where $\star$ stands for convolution and $L_1:=\max\{L_{m,b,a}\}$, where $L_{m,b,a}$ is the length of the T_c-sampled channel $h_{m,b,a}(k)$.

Casting (8) into a matrix form, we can express the ith transmitted block of the ath branch $u_{m,a}(i;p)$ of length N_1 by the $N_1\times 1$ vector

$$\mathbf{u}_{m,a}(i)=\mathbf{C}_m\beta_a\left(\mathbf{s}_m(i)\right) \quad (19)$$

where $\mathbf{s}_m(i) := [s_m(iK),\ldots,s_m((i+1)K-1)]^T$ is the $K\times 1$ vector representing the symbol block of length K with the following notational convention: $\beta_a(\mathbf{s}_m(i)) := [\beta_a(s_m(iK)),\ldots,\beta_a(s_m((i+1)K-1))]^T$ and $\mathbf{C}_m := [\mathbf{c}_{m,0}\ldots\mathbf{c}_{m,K-1}]$ denoting the $N_1\times K$ code matrix of user m with $k+1$th column $\mathbf{c}_{m,k} := [c_{m,k}(0),\ldots,c_{m,k}(N_1-1)]^T$.

At the mth receiver, according to the TDD-IRMA protocol in Section III, it suffices to collect the first $N_{L_1}:=N_1+L_1$ samples per transmitted burst to enable symbol recovery. The ith $N_{L_1}\times 1$ received block corresponding to the bth branch, defined as $\mathbf{y}_{m,b}(i) := [y_{m,b}(i(2N_1+L)),\ldots,y_{m,b}(i(2N_1+L)+N_{L_1}-1)]^T$, can be expressed as

$$\mathbf{y}_{m,b}(i)=\mathcal{P}\sum_{a=0}^{A-1}\mathbf{H}_{m,b,a}\mathbf{u}_{m,a}(i)+\boldsymbol{\eta}_b(i) \quad (20)$$

where $\boldsymbol{\eta}_b(i) := [\eta_b(i(2N_1+L)), \ldots, \eta_b(i(2N_1+L)+N_{L_1}-1)]^T$ and $\mathbf{H}_{m,b,a}$ are $N_{L_1} \times N_1$ Toeplitz convolution matrices given by

$$\mathbf{H}_{m,b,a} = \begin{pmatrix} h_{m,b,a}(0) & \cdots & 0 \\ \vdots & \ddots & \vdots \\ h_{m,b,a}(L_1) & & h_{m,b,a}(0) \\ \vdots & \ddots & \vdots \\ 0 & \cdots & h_{m,b,a}(L_1) \end{pmatrix}. \tag{21}$$

We can reexpress (20) for $b = 0, \ldots, A-1$ by defining the vectors of size $N_{L_1}A \times 1 \mathbf{y}_m(i) := [\mathbf{y}_{m,0}^T(i), \ldots, \mathbf{y}_{m,A-1}^T(i)]^T$ which leads to

$$\mathbf{y}_m(i) = \mathcal{P}\mathbf{H}_m\mathbf{u}_m(i) + \boldsymbol{\eta}(i) \tag{22}$$

where $\mathbf{u}_m(i) := [\mathbf{u}_{m,0}^T(i), \ldots, \mathbf{u}_{m,A-1}^T(i)]^T$, $\boldsymbol{\eta}(i) := [\boldsymbol{\eta}_0^T(i), \ldots, \boldsymbol{\eta}_{A-1}^T(i)]^T$, and $\mathbf{H}_m$ is a block $N_{L_1}A \times N_1A$ matrix given by

$$\mathbf{H}_m := \begin{pmatrix} \mathbf{H}_{m,0,0} & \mathbf{H}_{m,0,1} & \cdots & \mathbf{H}_{m,0,A-1} \\ \mathbf{H}_{m,1,0} & \mathbf{H}_{m,1,1} & \cdots & \mathbf{H}_{m,1,A-1} \\ \vdots & \vdots & \ddots & \vdots \\ \mathbf{H}_{m,A-1,0} & \mathbf{H}_{m,A-1,1} & \cdots & \mathbf{H}_{m,A-1,A-1} \end{pmatrix}. \tag{23}$$

The model in (20)–(23) is MIMO, but as we will see next, the discrete counterpart of the approximate model in Section II-C is SISO.

B. Oversampled SISO Model

Consider the modulated signal (12) propagating through a linear channel $h_m(t)$, corrupted by additive noise $\eta(t)$ and filtered at the receiver with the filter matched to the pulse $w(t)$. The resulting SISO model is shown in Fig. 8. Then, in order to obtain the discrete-time equivalent model of the approximate continuous-time PPM-IRMA, we sample the received signal at a rate $1/T_\tau$. The discrete-time equivalent channel is thus $h_m(n) := w(t) \star h_m(t) \star w(-t)|_{t=nT_\tau}$. Defining the noise $\eta(n) := \eta(t) \star w(-t)|_{t=nT_\tau}$, the discrete-time equivalent PPM-IRMA model is given by

$$\bar{y}_m(n) = \mathcal{P}\sum_{k=0}^{L_m} h_m(k)\bar{u}_m(n-k) + \eta(n) \tag{24}$$

where L_m is the length of the T_τ-sampled channel $h_m(n)$ and the sequence $\bar{u}_m(n)$ is given by (11).

Casting (10) into a matrix form, we can express the ith transmitted block of the ath branch $\bar{u}_{m,a}(i;p)$ by the $N_1' \times 1$ vector

$$\bar{\mathbf{u}}_{m,a}(i) = \bar{\mathbf{C}}_{m,a}\beta_a(\mathbf{s}_m(i)) \tag{25}$$

where $\mathbf{s}_m(i) := [s_m(iK), \ldots, s_m((i+1)K-1)]^T$ is the $K \times 1$ vector representing the symbol block of length K with the following notational convention: $\beta_a(\mathbf{s}_m(i)) := [\beta_a(s_m(iK)), \ldots, \beta_a(s_m((i+1)K-1))]^T$ and $\bar{\mathbf{C}}_{m,a} := [\bar{\mathbf{c}}_{m,a,0} \ldots \bar{\mathbf{c}}_{m,a,K-1}]$ is the $N_1' \times K$ code matrix for the spreading of branch a. Defining $\sigma_p(\cdot)$ as the downshift operator of order p for column vectors with zero padding for new entries, vectors $\bar{\mathbf{c}}_{m,a,k}$ can be expressed as $\bar{\mathbf{c}}_{m,a,k} := \sigma_{d_a}(\bar{\mathbf{c}}_{m,k})$

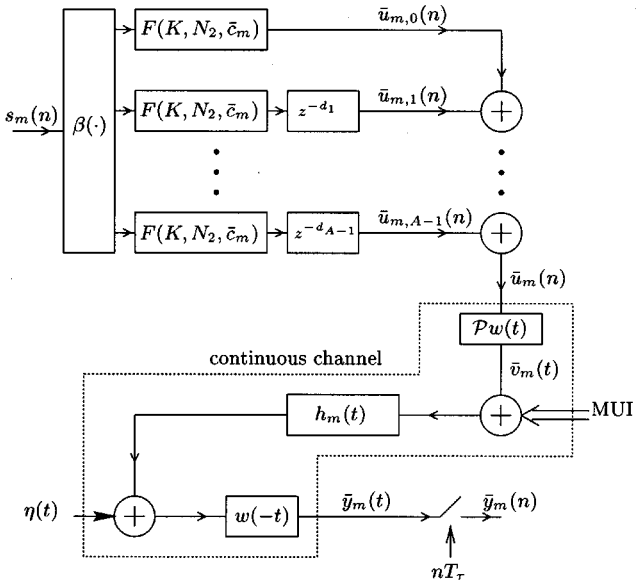

Fig. 8. SISO PPM-IRMA model for the downlink (mth user receiver).

with $\bar{\mathbf{c}}_{m,k} := [\bar{c}_{m,k}(0), \ldots, \bar{c}_{m,k}(N_1'-1)]^T$. Thus, using (25) we can cast (11) in vector form and the ith transmitted block for user m is given by $\bar{\mathbf{u}}_m(i) = \sum_{a=0}^{A-1} \bar{\mathbf{u}}_{m,a}$.

Because the sample rate has increased, the quantities L, L_1, L_2 defined for the TDD-IRMA protocol in Section III have to be modified accordingly. Thus, we define the equivalent T_τ-sampled duration for δ_1, δ_2 and L_{si} as $L_1' := \lceil(\delta_1 N_\tau)/T_c\rceil$, $L_2' := \lceil(\delta_2 N_\tau)/T_c\rceil$ and $L' := L_1' + L_2'$. Likewise, the number of trailing zeros for the code sequence has to be equal to $N_1' + L'$ and thus, the code length becomes $N_3' = 2N_1' + L'$.

At the mth receiver, it suffices to collect the first $N_{L_1}' := N_1' + L_1'$ samples per transmitted burst to enable symbol recovery. Then, the ith $N_{L_1}' \times 1$ received vector is defined as $\bar{\mathbf{y}}_m(i) := [\bar{y}_m(i(2N_1'+L')), \ldots, \bar{y}_m(i(2N_1'+L')+N_{L_1}'-1)]^T$. And, according to (24), $\bar{\mathbf{y}}_m(i)$ can be expressed as

$$\bar{\mathbf{y}}_m(i) = \mathcal{P}\bar{\mathbf{H}}_m\bar{\mathbf{u}}_m(i) + \bar{\boldsymbol{\eta}}(i) \tag{26}$$

where $\bar{\mathbf{H}}_m$ is an $(N_{L_1}' \times N_1')$ Toeplitz convolution matrix given by

$$\bar{\mathbf{H}}_m = \begin{pmatrix} h_m(0) & \cdots & 0 \\ \vdots & \ddots & \vdots \\ h_m(L_1') & & h_m(0) \\ \vdots & \ddots & \vdots \\ 0 & \cdots & h_m(L_1') \end{pmatrix} \tag{27}$$

and $\bar{\boldsymbol{\eta}}(i) := [\eta(i(2N_1'+L')), \ldots, \eta(i(2N_1'+L')+N_{L_1}'-1)]^T$.

We have seen that an approximation of the MIMO model leads to a SISO one which has lower complexity. It has one pulse-shaper for the transmitter and one receive-filter whereas the MIMO model needs A pulse-shapers and A receive filters. However, the price to pay for such a simplification is an increase of the sampling rate. If the pulses are equally spaced in time ($\tau_n = n(T_c/A)$, $0 \le n < A$), the SISO model is equal to the MIMO and the sampling rate is multiplied by A. Finally, we will see in the next section that the channel in the SISO model is always invertible, which is not true for the MIMO one.

As mentioned in Section II-D, the proposed TDD-IRMA model can also accommodate nonblock periodic codes. In this case, the spreading code matrix will be different from one burst to the next. They will have to be indexed by i, the burst number (block of K symbols). Thus the matrix $\mathbf{C}_m$ in (19) for the MIMO case and $\bar{\mathbf{C}}_{m,a}$ in (25) for the SISO case, will have to be replaced by matrices $\mathbf{C}_m([i]_{N_\ell})$ (resp. $\bar{\mathbf{C}}_{m,a}([i]_{N_\ell})$) with $N_\ell = \mathrm{LCM}(\mathrm{P_c}, \mathrm{KN_f})$ and $[i]_{N_\ell} = i \mathrm{mod} \mathrm{N}_\ell$. In the same way, the receivers developed in the next section will have to be modified accordingly.

V. Digital Receivers for the Downlink

We describe here three linear receivers for the downlink of a cellular multiuser scheme (see [16] and reference therein), using the TDD and the orthogonal code design described in Section III for both MIMO and SISO models. We assume that the known channel is time invariant, but adaptive variants of these receivers or successive interference cancellers can be also derived to handle slowly-varying channels. Although not considered here, nonlinear receivers such as DFEs (see, e.g., [16]) are also applicable.

Because PPM is a nonlinear modulation, the receivers will operate in two stages: 1) a linear filtering stage to eliminate channel effects and separate the users, and 2) a nonlinear processing stage to recover the symbols.

A. MIMO Model

The ith transmitted symbol block for the downlink is given by $\mathbf{u}(i) = \sum_{\mu=0}^{N_c-1} \mathbf{u}_\mu(i)$, while the received block at the mth receiver is

$$\mathbf{y}_m(i) = \mathcal{P}\mathbf{H}_m\mathbf{u}(i) + \boldsymbol{\eta}(i). \tag{28}$$

Based on the vector model (28), a multichannel finite-impulse response (FIR) receiver can be described by a matrix $\mathbf{G}_m$ of dimension $KA \times N_{L_1}A$ as follows: $\widehat{\boldsymbol{\beta}}_{\mathbf{s}_m(i)} = \mathbf{G}_m\mathbf{y}_m(i) = \mathcal{P}\mathbf{G}_m\mathbf{H}_m\mathbf{u}(i) + \breve{\boldsymbol{\eta}}(i)$, where $\widehat{\boldsymbol{\beta}}_{\mathbf{s}_m(i)} := [\widehat{\beta}_0^T(\mathbf{s}_m(i)), \ldots, \widehat{\beta}_{A-1}^T(\mathbf{s}_m(i))]^T$ is the $KA \times 1$ estimated vector of the symbols transformed by the nonlinear function $\beta(\cdot)$ and $\breve{\boldsymbol{\eta}}(i) := \mathbf{G}_m\boldsymbol{\eta}(i)$ is the filtered noise.

Depending on how we select $\mathbf{G}_m$, we obtain different *linear receivers* and possible choices include ZF, matched filter (MF), and MMSE. These receivers are given by the following:

ZF (a.k.a. Decorrelating) Receiver

$$\mathbf{G}_m^{\mathrm{ZF}} := \mathrm{diag}\left(\underbrace{\mathbf{C}_m^T, \ldots, \mathbf{C}_m^T}_{A}\right) \left(\mathbf{H}_m^T\mathbf{H}_m\right)^{-1} \frac{\mathbf{H}_m^T}{N_f}. \tag{29}$$

MF (a.k.a. Rake) Receiver

$$\mathbf{G}_m^{\mathrm{MF}} := \mathrm{diag}\left(\underbrace{\mathbf{C}_m^T, \ldots, \mathbf{C}_m^T}_{A}\right) \frac{\mathbf{H}_m^T}{N_f}. \tag{30}$$

MMSE Receiver

$$\mathbf{G}_m^{\mathrm{MMSE}} := \boldsymbol{\Gamma}_m\mathbf{H}_m^T \left[\boldsymbol{\Gamma}_{\boldsymbol{\eta}\boldsymbol{\eta}} + \mathbf{H}_m\mathbf{F}\mathbf{H}_m^T\right]^{-1} \tag{31}$$

where $\mathbf{F}$ is an $N_1A \times N_1A$ block matrix

$$\mathbf{F} := \begin{pmatrix} \mathbf{F}_{0,0} & \cdots & \mathbf{F}_{0,A-1} \\ \vdots & \ldots & \vdots \\ \mathbf{F}_{A-1,0} & \cdots & \mathbf{F}_{A-1,A-1} \end{pmatrix} \tag{32}$$

with $N_1 \times N_1$ blocks given by $\mathbf{F}_{p,q} := \sum_{k,\ell=0}^{N_c-1} \mathbf{C}_k\boldsymbol{\Gamma}_{p,k,q,\ell}\mathbf{C}_\ell^T$, where $\boldsymbol{\Gamma}_{p,k,q,\ell} := E[\beta_p(\mathbf{s}_k)\beta_q^T(\mathbf{s}_\ell)]$ is $K \times K$. Matrix $\boldsymbol{\Gamma}_{\boldsymbol{\eta}\boldsymbol{\eta}} := E[\boldsymbol{\eta}(i)\boldsymbol{\eta}^T(i)]$ is $N_{L_1} \times N_{L_1}$ and block matrix $\boldsymbol{\Gamma}_m$ is $KA \times N_1A$

$$\boldsymbol{\Gamma}_m := \begin{pmatrix} \boldsymbol{\Gamma}_{m,0,0} & \cdots & \boldsymbol{\Gamma}_{m,0,A-1} \\ \vdots & \ldots & \vdots \\ \boldsymbol{\Gamma}_{m,A-1,0} & \cdots & \boldsymbol{\Gamma}_{m,A-1,A-1} \end{pmatrix} \tag{33}$$

with $K \times N_1$ blocks given by $\boldsymbol{\Gamma}_{m,p,q} := \sum_{\mu=0}^{N_c-1} \boldsymbol{\Gamma}_{p,m,q,\mu}\mathbf{C}_\mu^T$.

Due to its structure, matrix $\mathbf{H}_m$ in (23) is not guaranteed to be full rank and therefore the ZF receiver (29) might not always exist.

As for symbol detection, assuming that the noise $\eta(t)$ is Gaussian, the optimal detector in the ML sense is given by $\widehat{\mathbf{s}}_m(i) = \arg\min_{\mathbf{s}} \|\widehat{\boldsymbol{\beta}}_{\mathbf{s}_m(i)} - \boldsymbol{\beta}_{\mathbf{s}}\|^2_{\boldsymbol{\Sigma}^{-1}}$ where $\boldsymbol{\Sigma} := E[\breve{\boldsymbol{\eta}}(i)\breve{\boldsymbol{\eta}}^T(i)] = \mathbf{G}_m\boldsymbol{\Gamma}_{\boldsymbol{\eta}\boldsymbol{\eta}}\mathbf{G}_m^T$ is the correlation matrix of the filtered noise $\breve{\boldsymbol{\eta}}(i)$.

B. SISO Model

For the downlink, the ith transmit block of symbols is given by $\bar{\mathbf{u}}(i) = \sum_{\mu=0}^{N_c-1} \bar{\mathbf{u}}_\mu(i)$, while the corresponding received block vector at the mth receiver is

$$\bar{\mathbf{y}}_m(i) = \mathcal{P}\bar{\mathbf{H}}_m\bar{\mathbf{u}}(i) + \bar{\boldsymbol{\eta}}(i). \tag{34}$$

Based on the vector model (34), a multichannel FIR receiver can be described by a matrix $\bar{\mathbf{G}}_m$ of dimension $AK \times N'_{L_1}$ as follows: $\widehat{\boldsymbol{\beta}}_{\mathbf{s}_m(i)} = \bar{\mathbf{G}}_m\bar{\mathbf{y}}_m(i) = \mathcal{P}\bar{\mathbf{G}}_m\bar{\mathbf{H}}_m\bar{\mathbf{u}}(i) + \breve{\bar{\boldsymbol{\eta}}}(i)$, where $\breve{\bar{\boldsymbol{\eta}}}(i) := \bar{\mathbf{G}}_m\bar{\boldsymbol{\eta}}(i)$ is the filtered noise. As for the MIMO model, depending on how we select $\bar{\mathbf{G}}_m$, we obtain similar to (29)–(31) different linear receivers.

ZF (a.k.a. Decorrelating) Receiver

$$\begin{aligned} \bar{\mathbf{G}}_m^{\mathrm{ZF}} &:= \left[\bar{\mathbf{Z}}_{m,0}^T, \ldots, \bar{\mathbf{Z}}_{m,A-1}^T\right]^T, \\ \bar{\mathbf{Z}}_{m,a} &:= \bar{\mathbf{C}}_{m,a}^T \left(\bar{\mathbf{H}}_m^T\bar{\mathbf{H}}_m\right)^{-1} \frac{\bar{\mathbf{H}}_m^T}{N_f}. \end{aligned} \tag{35}$$

MF (a.k.a. Rake) Receiver

$$\bar{\mathbf{G}}_m^{\mathrm{MF}} := \left[\bar{\mathbf{M}}_{m,0}^T, \ldots, \bar{\mathbf{M}}_{m,A-1}^T\right]^T, \quad \bar{\mathbf{M}}_{m,a} := \bar{\mathbf{C}}_{m,a}^T \frac{\bar{\mathbf{H}}_m^T}{N_f}. \tag{36}$$

MMSE Receiver

$$\bar{\mathbf{G}}_m^{\mathrm{MMSE}} := \bar{\boldsymbol{\Gamma}}_m\bar{\mathbf{H}}_m^T \left[\boldsymbol{\Gamma}_{\bar{\boldsymbol{\eta}}\bar{\boldsymbol{\eta}}} + \bar{\mathbf{H}}_m\bar{\mathbf{F}}\bar{\mathbf{H}}_m^T\right]^{-1} \tag{37}$$

where $\bar{\mathbf{F}} := \sum_{p,q=0}^{N_c-1} \sum_{k,\ell=0}^{A-1} \bar{\mathbf{C}}_{p,k}\boldsymbol{\Gamma}_{k,p,\ell,q}\bar{\mathbf{C}}_{q,\ell}^T$ is $N'_1 \times N'_1$, $\bar{\boldsymbol{\Gamma}}_m := [\bar{\boldsymbol{\Gamma}}_{0,m}^T, \ldots, \bar{\boldsymbol{\Gamma}}_{A-1,m}^T]^T$ is $AK \times N'_1$, $\bar{\boldsymbol{\Gamma}}_{a,m} := \sum_{\mu=0}^{N_c-1} \sum_{\alpha=0}^{A-1} \boldsymbol{\Gamma}_{a,m,\alpha,\mu}\bar{\mathbf{C}}_{\mu,\alpha}^T$ is $K \times N'_1$, and $\boldsymbol{\Gamma}_{\bar{\boldsymbol{\eta}}\bar{\boldsymbol{\eta}}} := E[\bar{\boldsymbol{\eta}}(i)\bar{\boldsymbol{\eta}}^T(i)]$ is $N'_{L_1} \times N'_{L_1}$.

Inasmuch as $\bar{\mathbf{H}}_m$ is Toeplitz and the impulse response $\{h_m(n)\}_{n=0}^{L'_1}$ has at least one nonzero value, $\bar{\mathbf{H}}_m^T\bar{\mathbf{H}}_m$ has full rank N'_1 and is thus always invertible. As a consequence, the channel is always invertible. We infer that for the ZF receiver, MUI is canceled due to the orthogonality among spreading

codes. Specifically, since $\bar{\mathbf{C}}_{m_1,a_1}^T \bar{\mathbf{C}}_{m_2,a_2} = N_f \cdot \delta_{m_1,m_2}\delta_{a_1,a_2}\mathbf{I}$, we have (assuming $\mathcal{P} = 1$)

$$\begin{aligned}\bar{\mathbf{Z}}_{m,a}\bar{\mathbf{y}}_m(i) &= \frac{1}{N_f}\bar{\mathbf{C}}_{m,a}^T \left(\bar{\mathbf{H}}_m^T\bar{\mathbf{H}}_m\right)^{-1}\bar{\mathbf{H}}_m^T\bar{\mathbf{H}}_m\bar{\mathbf{u}}(i) + \bar{\mathbf{Z}}_{m,a}\bar{\boldsymbol{\eta}}(i)\\ &= \frac{1}{N_f}\bar{\mathbf{C}}_{m,a}^T \sum_{\mu=0}^{N_c-1}\sum_{\alpha=0}^{A-1}\bar{\mathbf{C}}_{\mu,\alpha}\beta_\alpha\left(\mathbf{s}_\mu(i)\right) + \bar{\mathbf{Z}}_{m,a}\bar{\boldsymbol{\eta}}(i)\\ &= \beta_a\left(\mathbf{s}_m(i)\right) + \bar{\mathbf{Z}}_{m,a}\bar{\boldsymbol{\eta}}(i). \end{aligned} \tag{38}$$

Thus, equalizer $\bar{\mathbf{G}}_m^{\mathrm{ZF}}$ achieves (almost) error-free symbol recovery in the noise-free (high SNR) case, regardless of the channel. One can remark that the MIMO model does not hold this property, since matrix $\mathbf{H}_m$ in (29) may not always be guaranteed to have full rank although it is a rare event.

As for symbol detection, assuming that the noise $\eta(t)$ is Gaussian, the optimal detector in the ML sense is given by $\hat{\mathbf{s}}_m(i) = \arg\min_{\mathbf{s}} \|\hat{\boldsymbol{\beta}}_{\mathbf{s}_m(i)} - \boldsymbol{\beta}_{\mathbf{s}}\|^2_{\bar{\boldsymbol{\Sigma}}^{-1}}$ with $\bar{\boldsymbol{\Sigma}} := \bar{\mathbf{G}}_m\boldsymbol{\Gamma}_{\bar{\boldsymbol{\eta}}\bar{\boldsymbol{\eta}}}\bar{\mathbf{G}}_m^T$.

We have derived three linear receivers for both MIMO and SISO models. We have assumed that the channel was known, which that can be obtained for instance by using probe sequences within the information symbols.

We will now give a SER bound for the ZF receiver and show some simulations of the different receivers.

VI. Performance

We first derive an upper bound on the SER for the ZF receiver and then present a simulation example of the proposed downlink TDD-PPM-IRMA scheme in a multipath environment for both MIMO and SISO models.

A. SER Bound for the ZF Receiver

Because the linear stage of the ZF receiver cancels the effect of the channel and the MUI, we can derive an upper bound for the SER. We present here the derivation using the MIMO receiver for simplicity, but the resulting expression is identical for the SISO as well. Provided that the matrix $\mathbf{H}_m$ is invertible in (28), the output of the linear filter (29) can be expressed as $\hat{\boldsymbol{\beta}}_{s_m} = \boldsymbol{\beta}_{s_m} + \mathbf{G}_m^{\mathrm{ZF}}\boldsymbol{\eta}$. Then, given the symbol $\mathbf{s}_m$, the error probability for the ML detector is given by $P_e(\mathbf{s}_m) = \Pr\{\bigcup_{\mathbf{s}\in\mathcal{A}_{\mathbf{s}}\setminus\mathbf{s}_m} \boldsymbol{\delta}_{\mathbf{s}}^T\boldsymbol{\Sigma}^{-1}\boldsymbol{\delta}_{\mathbf{s}} + 2\boldsymbol{\eta}^T(\mathbf{G}_m^{\mathrm{ZF}})^T\boldsymbol{\Sigma}^{-1}\boldsymbol{\delta}_{\mathbf{s}} < 0\}$, where $\mathcal{A}_{\mathbf{s}}$ is the set of all possible symbol vectors $\mathbf{s}$ and $\boldsymbol{\delta}_{\mathbf{s}} := \boldsymbol{\beta}_{\mathbf{s}_m} - \boldsymbol{\beta}_{\mathbf{s}}$. Introducing the notation $d_{\mathbf{s}} = \boldsymbol{\delta}_{\mathbf{s}}^T\boldsymbol{\Sigma}^{-1}\boldsymbol{\delta}_{\mathbf{s}}$ and $\mathbf{v}_{\mathbf{s}} = 2(\mathbf{G}_m^{\mathrm{ZF}})^T\boldsymbol{\Sigma}^{-1}\boldsymbol{\delta}_{\mathbf{s}}$, the probability of error can be approximated using the *union bound* by $P_e(\mathbf{s}_m) \leq \sum_{\mathbf{s}\in\mathcal{A}_{\mathbf{s}}\setminus\mathbf{s}_m}\Pr\left\{d_{\mathbf{s}}(\mathbf{s}_m) + \boldsymbol{\eta}^T\mathbf{v}_{\mathbf{s}} < 0\right\}$. In the latter expression $d_{\mathbf{s}}(\mathbf{s}_m)$ is a constant and $\boldsymbol{\eta}^T\mathbf{v}_{\mathbf{s}}$ is a random Gaussian variable with zero mean and variance equal to $\sigma^2 = \mathbf{v}_{\mathbf{s}}^T\mathbf{v}_{\mathbf{s}}\sigma_\eta^2$, where $\sigma_\eta^2 = E[\eta^2(n)]$; hence, we find $\Pr\left\{d_{\mathbf{s}}(\mathbf{s}_m) + \boldsymbol{\eta}^T\mathbf{v}_{\mathbf{s}} < 0\right\} = 1/2\mathrm{erfc}(\mathrm{d_s(s_m)}/(\sqrt{2\mathbf{v}_{\mathbf{s}}^T\mathbf{v}_{\mathbf{s}}}\sigma_\eta))$.

Assuming the symbols to be equally probable, we can then deduce the following expression for the SER bound:

$$\mathrm{SER} \leq 1 - \left(1 - \frac{1}{2A^K}\sum_{\mathbf{s}_i\in\mathcal{A}_{\mathbf{s}}}\sum_{\mathbf{s}\in\mathcal{A}_{\mathbf{s}}\setminus\mathbf{s}_i}\mathrm{erfc}\left(\frac{d_{\mathbf{s}}(\mathbf{s}_i)}{\sqrt{2\mathbf{v}_{\mathbf{s}}^T\mathbf{v}_{\mathbf{s}}}\sigma_\eta}\right)\right)^{1/K}. \tag{39}$$

B. Simulations

We present here simulations to illustrate the behavior of the different receivers. The selected configuration is a binary PPM modulation ($q_A = 1$), eight users ($N_c' = 8$) and two symbols per burst ($K = 2$). As per [10], we have chosen a frame duration $T_f = 100$ ns ns and a maximum delay spread equal to 100 ns. We have assumed a time guard of duration T_c; hence, $N_g = 1$. Thus, we deduce the chip duration $T_c = T_f/(N_c' + N_g) = 11.11$ ns. For the MIMO model, the sampling rate is equal to T_c which leads to a channel of length $L_1 = 9$ (assuming $l_m = 0$). Moreover, assuming $\tau_0 = 0$ and $\tau_1 = T_c/2$, the SISO model is obtained for $N_\tau = 2$ which leads then to a channel length $L_1' = 18$.

The channel is modeled by the Saleh–Valenzuela model [11], [17] for indoor IR systems with the same parameters. This model is based on clusters of rays. The received signal is composed of attenuated and delayed versions of the transmitted signal arriving in clusters. The times of arrival are modeled as a Poisson process and the amplitudes as Gaussian. For the simulations, the receivers will be assumed to be synchronized on the strongest path.

In the PPM-IRMA system, the received signal is the second derivative of the Gaussian function $\sqrt{\tau^3/3}(2/\pi)^{1/4}\exp(-t^2/\tau^2)$ (normalized to have $r_w(0) = 1$); hence, we have $r_w(t) = \exp(-t^2/(2\tau^2))[1 - 2(t/\tau)^2 + (t/\tau)^4/3]$, where $r_w(t)$ is the correlation function of $w(t)$ and the parameter $\tau = 0.1225$ ns is adjusted to yield a pulsewidth equal to 0.7 ns (see, e.g., [15]).

Fig. 9 depicts the BER corresponding to the three receivers for one channel trial and different values for N_f. We can see that the RAKE receiver performs poorly and exhibits a BER floor at high SNR. The MMSE performs the best while the ZF remains close to the MMSE. Fig. 9(a) shows that the BER of the ZF receiver is very close to the bound given by (39). Fig. 9(b) shows that, compared to Fig. 9(a), increasing the number of frames N_f improves slightly the performance for the ZF and MMSE receivers, but does not change their relative behavior. Moreover, it shows that for $N_f > 15$, the performance does not improve any more and thus, increasing N_f further does not provide any benefit.

Fig. 10 shows the average BER of the three receivers over 100 Monte Carlo channel realizations and for the same parameters as in Fig. 9(a). It shows that the behavior of the receivers remains the same and that the difference between the MMSE and ZF increases.

Simulations of the conventional IRMA (not shown here) were performed and confirmed the conclusion of [11], where even single-user performance was seen to suffer severely in the presence of multipath.

VII. Conclusion

An all-digital IR scheme was developed for ultra wideband multiple-access wireless cellular systems. It included a novel modeling of the conventional time-continuous IR along with a TDD protocol and orthogonal user code design. A discrete-time MIMO model was derived from the continuous-time one, along with an SISO approximate of it that turns out to have lower

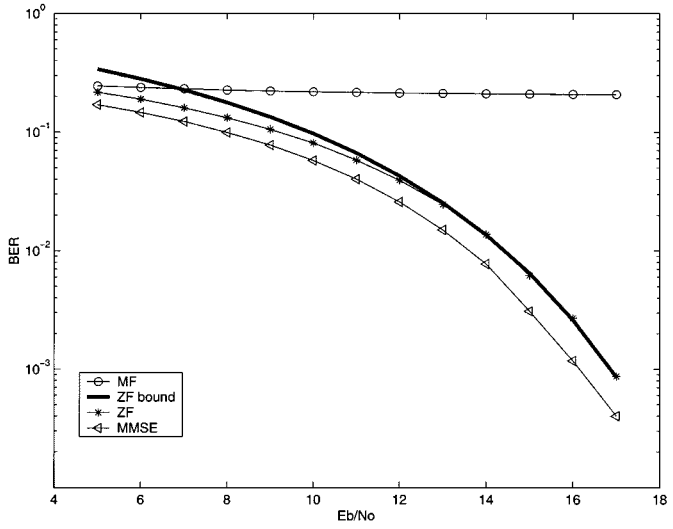

(a)

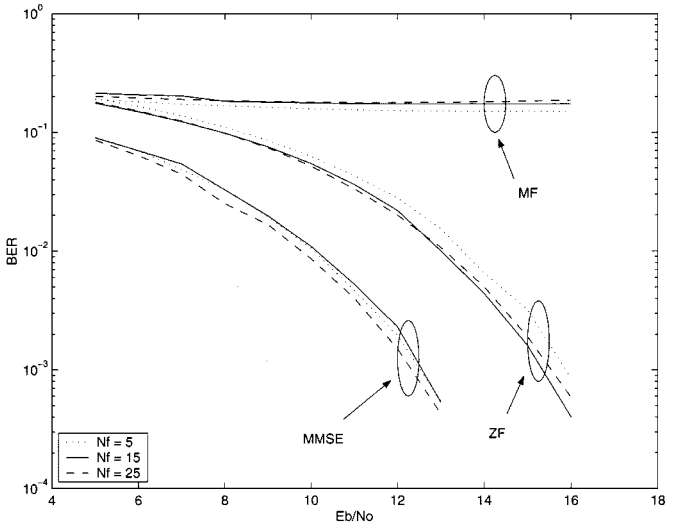

(b)

Fig. 9. Comparing the different receivers (ZF, MF, MMSE) for the binary PPM-IRMA scheme (MIMO model) with $K = 2$, $T_g = 1$ and 8 users. (a) For $N_f = 1$. Bound in (39) is plotted for the ZF receiver; (b) For $N_f = 5$, $N_f = 15$, and $N_f = 25$.

complexity, but operates at a higher sampling rate. Three linear receivers were also derived for the downlink (MF, ZF, MMSE), and for the SISO model it was shown that the decorrelating (ZF) receiver always exists, regardless of the channel zeros. An upper bound on the BER for the ZF receiver was derived and was found to be very close to the simulation.

Simulations of the three receivers were provided in a multiuser, frequency selective multipath channel environment, showing the different features for a given channel and over multipath channel realizations. It has been verified that the MF receiver performs poorly and exhibits a BER floor at high SNR. The MMSE performs the best while the ZF remains close the to MMSE. The simulations show clearly the benefit of multiuser detection over the conventional and the RAKE receivers. Moreover, it has been shown that increasing the number of frames per symbol N_f beyond a given threshold does not improve the performance. This suggests an optimal

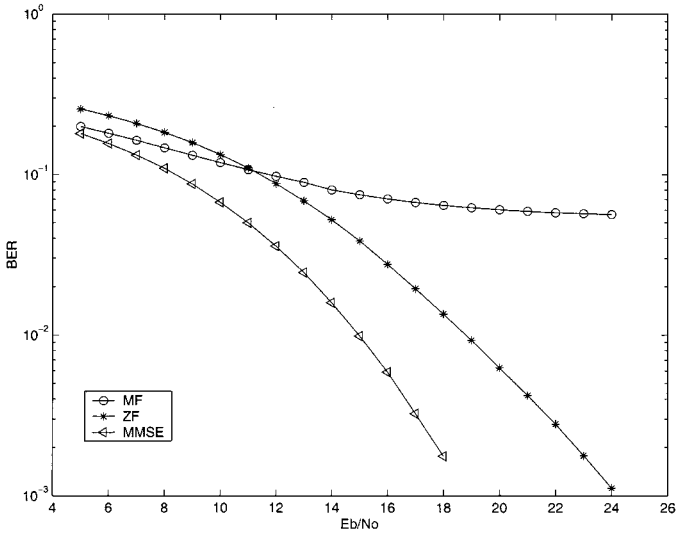

Fig. 10. Comparing the different receivers (ZF, MF, MMSE) for the PPM-IRMA scheme (MIMO model) for 100 Monte Carlo channel trials with the same parameters as in Fig. 9(a) .

value for N_f maximizing the data rate D, since D is inversely proportional to N_f (for a given T_f). However, peak power constraints would have to be taken into account for practical systems. Because equalization (with channel estimation) is not dedicated to one specific channel, the proposed receivers can be applied to other kinds of multipath channels that may be encountered in a cellular environment (such as those with longer multipath delay spread than the indoor model).

ACKNOWLEDGMENT

The authors would like to thank L. Yang for her comments on the revised version of this paper.

REFERENCES

[1] P. Withington II and L. W. Fullerton, "An impulse radio communications system," in *Proc. Int. Conf. on Ultra-Wide Band, Short-Pulse Electromagnetics*, Brooklyn, NY, Oct. 1992, pp. 113–120.

[2] R. A. Scholtz, "Multiple access with time-hopping impulse radio," in *Proc. Milcom Conf.*, Boston, MA, Oct. 1993, pp. 447–450.

[3] M. Z. Win and R. A. Scholtz, "On the energy capture of ultrawide bandwidth signals in dense multipath environments," *IEEE Commun. Lett.*, vol. 2, pp. 245–247, Sept. 1998.

[4] ——, "On the robustness of ultrawide bandwidth signals in dense multipath environments," *IEEE Commun. Lett.*, vol. 2, pp. 51–53, Feb. 1998.

[5] ——, "Ultrawide bandwidth time-hopping spread-spectrum impulse radio for wireless multiple-access communications," *IEEE Trans. Commun.*, vol. 48, pp. 679–691, Apr. 2000.

[6] F. Ramirez-Mireles, M. Z. Win, and R. A. Scholtz, "Signal selection for the indoor wireless impulse radio channel," in *Proc. 47th Vehicular Technology Conf.*, Phoenix, AZ, May 1997, pp. 2243–2247.

[7] F. Ramirez-Mireles and R. A. Scholtz, "N-orthogonal time-shift-modulated signals for ultrawideband impulse radio modulation," in *Proc. Globecom*, Phoenix, AZ, Nov. 1997, pp. 6–11.

[8] S. S. Kolenchery, K. Townsend, J. A. Freebersyser, and G. Bilbro, "Performance of local power control in peer-to-peer impulse radio networks with bursty traffic," in *Proc. Globecom*, Phoenix, AZ, Nov. 1997, pp. 910–916.

[9] S. S. Kolenchery, K. Townsend, and J. A. Freebersyser, "A novel impulse radio network for tactical wireless communications," in *Proc. Milcom*, Bedford, MA, Oct. 1998, pp. 59–65.

[10] M. Z. Win, X. Qiu, R. A. Scholtz, and V. O. K. Li, "ATM-based TH-SSMA network for multimedia PCS," *IEEE J. Select. Areas Commun.*, vol. 17, pp. 824–836, May 1999.

[11] Y. Shin, H. Lee, B. Han, and S. Im, "Multipath characteristics of impulse radio channel," in *Proc. 50th Vehicular Technology Conf.*, Boston, MA, Oct. 2000, pp. 2487–2491.
[12] Z. Wang and G. B. Giannakis, "Wireless multicarrier communications: Where Fourier meets Shannon," *IEEE Signal Processing Mag.*, vol. 17, no. 3, pp. 29–48, May 2000.
[13] A. L. Johansson and A. Svensson, "On multirate DS-CDMA schemes with interference cancellation," *J. Wireless Pers. Commun.*, vol. 9, pp. 1–29, Jan. 1999.
[14] G. B. Giannakis, Z. Wang, A. Scaglione, and S. Barbarossa, "AMOUR—Generalized multicarrier transceivers for blind CDMA irrespective of multipath," *IEEE Trans. Commun.*, vol. 48, pp. 2064–2076, Dec. 2000.
[15] M. Z. Win and R. A. Scholtz, "Impulse radio: How it works," *IEEE Commun. Lett.*, vol. 2, pp. 36–38, Feb. 1998.
[16] S. Verdú, *Multiuser Detection*. Cambridge, U.K.: Cambridge Univ. Press, 1998.

Christophe J. Le Martret was born in Rennes, France, on March 12, 1963. He received the Ph.D. degree from l'Université de Rennes 1, Rennes, France, in 1990.

From 1991 to 1995 he was with the CESTA, Bruz, France, and from 1996 to 2002 with the Centre d'Électronique de L'ARmement (CELAR). He has recently joined the Signal Processing Department, THALES Communications France, Genneviliers, France. He was a Visiting Researcher at SpinCom Laboratory, Department of ECE, University of Minnesota, Minneapolis, from 1999 to 2000. He has been teaching digital communications at École d'Ingénieurs Louis de Broglie, Bruz, France, since 1998. His current research interests are in statistical signal processing and communications: modulation classification, equalization, multiuser detection, and ultrawideband communications.

Georgios B. Giannakis (S'84–M'86–SM'91–F'97) received the Diploma in electrical engineering from the National Technical University of Athens, Greece, in 1981. He received the MSc. degree in electrical engineering in 1983, M.Sc. degree in mathematics in 1986, and the Ph.D. degree in electrical engineering in 1986, from the University of Southern California (USC), Los Angeles.

After lecturing for one year at USC, he joined the University of Virginia, Charlottesville, in 1987, where he became a Professor of Electrical Engineering in 1997. Since 1999, he has been a Professor with the Department of Electrical and Computer Engineering at the University of Minnesota, Minneapolis, where he now holds an ADC Chair in Wireless Telecommunications. His general interests span the areas of communications and signal processing, estimation and detection theory, time-series analysis, and system identification, subjects on which he has published more than 140 journal papers, 270 conference papers, and two books. Current research topics focus on transmitter and receiver diversity techniques for single- and multiuser fading communication channels, precoding and space-time coding for block transmissions, multicarrier, and wide-band wireless communication systems.

Dr. Giannakis is the co-recipient of four best paper awards from the IEEE Signal Processing (SP) Society (1992, 1998, 2000, 2001). He also received the Society's Technical Achievement Award in 2000. He co-organized three IEEE-SP Workshops, and guest co-edited four special issues. He has served as Editor in Chief for the IEEE SIGNAL PROCESSING L ETTERS, as Associate Editor for the IEEE TRANSACTIONS ON SIGNAL PROCESSING and the IEEE SIGNAL PROCESSING L ETTERS, as secretary of the SP Conference Board, as member of the SP Publications Board, as member and vice-chair of the Statistical Signal and Array Processing Technical Committee, and as chair of the SP for Communications Technical Committee. He is a member of the Editorial Board for the PROCEEDINGS OF THE IEEE, and the steering committee of the IEEE TRANSACTIONS ON WIRELESS COMMUNICATIONS. He is a member of the IEEE Fellows Election Committee, the IEEE-SP Society's Board of Governors, and is a frequent consultant for the telecommunications industry.